Inorganic Chemistry

Article

pubs.acs.org/IC

Lanthanide Dinuclear Complexes Involving Tetrathiafulvalene-3-pyridine-N-oxide Ligand: Semiconductor Radical Salt, Magnetic, and Photophysical Studies

Fabrice Pointillart,*,† Boris Le Guennic,† Olivier Maury,‡ Stéphane Golhen,† Olivier Cador,† and Lahcène Ouahab†

†Institut des Sciences Chimiques de Rennes, UMR 6226 CNRS, Université de Rennes 1, 263 Avenue du Général Leclerc, 35042 Rennes Cedex, France

‡Laboratoire de Chimie, UMR 5182 CNRS-ENS, Lyon-Université Lyon 1, 46 Allée d'Italie, 69364 Lyon Cedex 07, France

S *Supporting Information*

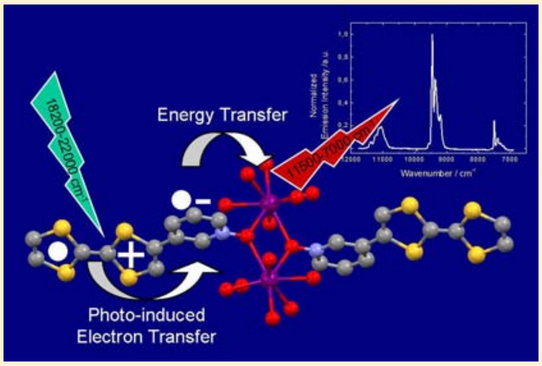

ABSTRACT: Centro-symmetric dinuclear complexes of formula [Ln(tta)$_3$(**L**)]$_2$·xCH$_2$Cl$_2$, (tta$^-$ = 2-thenoyltrifluoroacetonate anion, x = 0.5 for Ln = Eu (**1a**), Tb (**3**), and Dy (**4**) and x = 0 for Ln = Eu (**1b**) and Nd (**2**)) have been synthesized using the tetrathiafulvalene-3-pyridine-*N*-oxide as a bridging ligand (**L**). X-ray structures have shown the formation of channels with CH$_2$Cl$_2$ solvent inside. **1** is stable with both filled channels (at 150 K) and empty channels (at room temperature). The Dy^{III} analogue displays a complex butterfly like hysteresis loop at 1.5 K. Photophysical properties of the coordination complexes have been studied by solution and solid-state absorption spectroscopy. Time-dependent density functional theory (TD-DFT) calculations have been carried out on the diamagnetic Y^{III} derivative to shed light on the absorption spectrum. For **2**, the excitation of the charge transfer transitions induces line shape emission in the near-infrared spectral range assigned to $^4F_{3/2} \rightarrow {}^4I_{9/2}$, $^4F_{3/2} \rightarrow {}^4I_{11/2}$, and $^4F_{3/2} \rightarrow {}^4I_{13/2}$ neodymium centered transitions. The reversible redox-activity of the ligand **L** makes possible an original sensitization process involving a ligand centered charge separation followed by energy transfer to the Nd^{III} ion upon recombination.

■ INTRODUCTION

Since the discovery of the tetrathiafulvalene (TTF) in 1973,[1] many interesting materials based on this moiety have been obtained as organic metals, semiconductors, superconductors, magnets, and so forth.[2] In the past decade, TTF derivatives have been associated with d metal ions to elaborate multifunctional materials which possess magnetic and electrical properties.[2] It is only recently that the TTF-based ligands have been coordinated to 4f elements in order to exploit their particular properties.[3]

Such a research project was stimulated by the great magnetic moment and strong magnetic anisotropy of lanthanides that make them good candidates for the elaboration of Single Molecule Magnets (SMMs). SMMs have received much attention since their slow magnetization relaxation[4] makes them potentially suitable for magnetic storage, molecular spintronics, or quantum computing devices.[5] To obtain pure 4f SMMs, the most used 4f ion is without a doubt Dy^{III} [6] and to a lesser extent Tb^{III}.[7] The association of the former with TTF derivatives has led to SMM[3f] and Single Ion Magnet (SIM)[3i] behaviors.

On the other hand, lanthanides are widely studied for their specific luminescence properties.[8] Owing to the weak absorption of the forbidden f–f transitions, the lanthanide emission is usually sensitized by organic antenna chromophores which strongly absorb the UV–visible light and whose triplet state matches the accepting level of the lanthanide ion that an efficient energy transfer occurs.[9] Following the discovery that charge transfer excited states are able to directly sensitize Ln^{III} emission,[9e−g] a few research groups have demonstrated that TTF ligands could play such a role of antenna in the case of near-infrared (NIR) emitters such as Nd^{III},[10] Er^{III},[3h] and Yb^{III}.[3a,b,e] The interest for these ions comes from the significant technological applications of their luminescence in areas ranging from medical imaging to optical communications.[11] In this optic, complexes based on these ions are proposed as potential sensitive probes for fluoroimmunoassay tests due to the transparency of the biofluid in the NIR region.[12] In the particular case of Yb^{III}, it has been demonstrated that the sensitization process can involve a separated-charge [TTF$^{\bullet+}$-A-Yb^{II}] state (where A is an acceptor).[3a] Conversely, when the TTF-A dyad is not coordinated or coordinated to a metal other than Yb^{III}, a photoinduced separated-charge [TTF$^{\bullet+}$-A$^{\bullet-}$]* state can be formed. This is indeed what has been observed for the TTF-CH═CH-BTA ligand (where BTA is the 1,3-

Received: September 27, 2012
Published: January 22, 2013

benzothiazole ring).[13] This ligand has played a key role in the realization of fluorescence quenching phenomena and photocurrent generation.[14]

We recently reported the SMM behavior of the $[Dy(tta)_3(\mathbf{L})]_2{\cdot}x CH_2Cl_2$ complex (**4**) featuring two Dy^{III} ions bridged by the tetrathiafulvalene-3-py-*N*-oxide ligand (**L**; Scheme 1) with a relaxation energy barrier of 87(1) K.[3f] As a continuation of this preliminary study, we report herein additional magnetic measurements on this Dy^{III} derivative (**4**) and detailed studies of the whole family $[Ln(tta)_3(\mathbf{L})]_2{\cdot}x CH_2Cl_2$, ($tta^-$ = 2-thenoyltrifluoroacetonate anion, x = 0.5 for Ln = Eu (**1a**) and Tb (**3**), and x = 0 for Ln = Eu (**1b**) and Nd (**2**)). We previously reported the antenna effect of a TTF ligand involving a pyridine-*N*-oxide acceptor covalently linked by an amido bridge for the near-infrared luminescence. It could be interesting to observe the influence of the suppression of this chemical bridge on the physical properties. The crystal structure of the Eu^{III} derivative (**1**) has been resolved at both 150 K (**1a**) and room temperature (**1b**) to study the structural changes. The photophysical properties of the Nd^{III} derivative (**2**) have been experimentally and theoretically studied with particular attention to the description of the sensitization process. The magnetic properties of the Nd^{III} and Tb^{III} have been determined. Finally, first attempts to electrocrystallize these compounds in order to reach electronic conductivity have been made.

Scheme 1. Representation of L and tta^- Anion

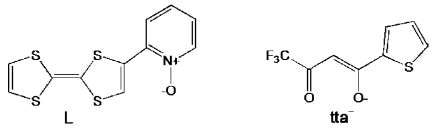

Table 1. X-Ray Crystallographic Data for the Radical Salt $L^{\bullet+}BF_4^-$ and Complexes 1−3

compounds	$[Eu(tta)_3(\mathbf{L})]_2{\cdot}0.5CH_2Cl_2$ (**1a**)	$[Eu(tta)_3(\mathbf{L})]_2$ (**1b**)	$[\mathbf{L}(BF_3)]{\cdot}0.5[(BF_4)(BF_3)]$ ($\mathbf{L}^{\bullet+}\mathbf{BF_4}^-$)
formula	$C_{70.5}H_{39}Cl_1Eu_2F_{18}N_2O_{14}S_{14}$	$C_{70}H_{38}Eu_2F_{18}N_2O_{14}S_{14}$	$C_{11}H_7B_2F_{6.5}N_1O_1S_4$
M/g·mol^{-1}	2266.5	2224.0	442.6
cryst syst	monoclinic	monoclinic	orthorhombic
space group	$P2_1/n$ (No. 14)	$P2_1/n$ (No. 14)	$Pnaa$ (No. 56)
cell params	a = 14.1053(3) Å	a = 14.3160(2) Å	a = 12.3485(5) Å
	b = 18.1336(4) Å	b = 18.2710(5) Å	b = 13.4518(11) Å
	c = 18.9155(5) Å	c = 18.9730(5) Å	c = 19.6002(15) Å
	β = 103.2343(10)°	β = 103.876(5)°	
volume/Å^3	4709.7(3)	4817.7(2)	3255.8(4)
cell formula units	2	2	4
T/K	150(2)	293(2)	293(2)
diffraction refln	$5.56 \leq 2\theta \leq 54.54$	$3.68 \leq 2\theta \leq 54.72$	$3.68 \leq 2\theta \leq 52.08$
ρ_{calc}, g·cm^{-3}	1.598	1.534	1.806
μ, mm^{-1}	1.749	1.681	0.653
number of reflns	40067	36038	11258
independent reflns	10701	10727	3165
$F_o^2 > 2\sigma(F_o)^2$	8331	6816	2028
number of variables	614	605	250
R_{int}, R_1, wR_2	0.0329, 0.0558, 0.1803	0.0480, 0.0620, 0.1674	0.0741, 0.0628, 0.1655

compounds	$[Nd(tta)_3(\mathbf{L})]_2$ (**2**)	$[Tb(tta)_3(\mathbf{L})]_2{\cdot}0.5CH_2Cl_2$ (**3**)
formula	$C_{70}H_{38}Nd_2F_{18}N_2O_{14}S_{14}$	$C_{70.5}H_{39}Cl_1Tb_2F_{18}N_2O_{14}S_{14}$
M/g·mol^{-1}	2208.5	2280.3
cryst syst	monoclinic	monoclinic
space group	$P2_1/n$ (No. 14)	$P2_1/n$ (No. 14)
cell params	a = 14.2823(3) Å	a = 14.0934(6) Å
	b = 18.3520(6) Å	b = 18.0179(8) Å
	c = 19.0377(6) Å	c = 18.7426(8) Å
	β = 103.845(2)°	β = 103.0129(15)°
volume/Å^3	4844.9(2)	4637.1(5)
cell formula units	Z = 2	Z = 2
T/K	293(2)	150(2)
diffraction refln	$4.44° \leq 2\theta \leq 53.46°$	$3.18° \leq 2\theta \leq 55.00°$
ρ_{calc}, g·cm^{-3}	1.515	1.635
μ, mm^{-1}	1.449	1.949
number of reflns	20032	38325
independent reflns	10208	10653
$F_o^2 > 2\sigma(F_o)^2$	6668	7667
number of variables	605	617
R_{int}, R_1, wR_2	0.0285, 0.0604, 0.1642	0.0431, 0.0540, 0.1712

■ EXPERIMENTAL SECTION

General Procedures and Materials. All solvents were dried using standard procedures. $Ln(tta)_3 \cdot 2H_2O$[15] and tetrathiafulvalene-3-pyridine-*N*-oxide (**L**)[3f] are prepared according to the literature procedure. All other reagents were purchased from Aldrich Co. Ltd. and were used without further purification. The preparation of $[Dy(tta)_3(L)]_2 \cdot 0.5CH_2Cl_2$ was reported before.[3f]

$[Ln(tta)_3(L)]_2 \cdot xCH_2Cl_2$, x = 0.5 for Ln = Eu (1a) and Tb (3) and x = 0 for Ln = Eu (1b) and Nd (2). $Ln(tta)_3 \cdot 2H_2O$ (0.04 mmol) is dissolved in 5 mL of CH_2Cl_2 and added to a solution of 5 mL of CH_2Cl_2 containing **L** (11.9 mg, 0.04 mmol). The solution is stirred for 15 min, and then *n*-hexane is layered to give dark red single crystals of **1**−**3**. Yield: 64 mg (72%) for **1**, 73 mg (83%) for **2**, and 37 mg (42%) for **3**. Anal. Calcd (%) for $C_{70}H_{38}N_2O_{14}S_{14}F_{18}Eu_2$: C, 37.77; H, 1.71; N, 1.26. Found: C, 37.46; H, 1.79; N, 1.29. Anal. Calcd (%) for $C_{70}H_{38}N_2O_{14}S_{14}F_{18}Nd_2$: C, 38.04; H, 1.72; N, 1.27. Found: C, 38.06; H, 1.71; N, 1.19. Anal. Calcd (%) for $C_{70}H_{38}N_2O_{14}S_{14}F_{18}Tb_2$: C, 37.54; H, 1.70; N, 1.25. Found: C, 37.66; H, 1.81; N, 1.21. Typical I.R spectra (KBr): ν 3113, 3040, 1652, 1604, 1540, 1507, 1475, 1437, 1413, 1356, 1311, 1248, 1231, 1187, 1140, 1062, 936, 859, 787, 642, 583 cm^{-1}. The formula for elemental analysis takes into account that the solvent molecules of crystallization were gone for **1a** and **3**.

$[L(BF_3)]_2^{\bullet+}[(BF_4)(BF_3)]^-$ ($L^{\bullet+}BF_4^-$). Suitable X-ray diffraction black block crystals of $\mathbf{L^{\bullet+}BF_4^-}$ were obtained by the galvanostatic (I = 5 μA) oxidation of **2** (22 mg) under an argon atmosphere at 293(2) K after 10 weeks, using $(Bu_4N)(BF_4)$ (200 mg) in CH_2Cl_2 (20 mL) as electrolytes. Platinum electrodes of about 2 cm in length and 1 mm in diameter were used for this electrocrystallization. Yield (single crystals): 4.3 mg (44%).

Crystallography. Single crystals of **1b**, **2**, and $\mathbf{L^{\bullet+}BF_4^-}$ were mounted on a Nonius four circle diffractometer equipped with a CCD camera and a graphite monochromated Mo Kα radiation source (λ = 0.71073 Å), while single crystals of **1a** and **3** were picked up with a cryoloop and then frozen at T = 150 K under a stream of dry N2 on a APEXII Bruker-AXS diffractometer for data collection from the Centre de Diffractométrie (CDIFX), Université de Rennes 1, France. Structures were solved with a direct method using the SIR-97 program and refined with a full matrix least-squares method on F^2 using the SHELXL-97 program.[16] Crystallographic data are summarized in Table 1. The checkcifs for both X-ray structures made at room temperature listed some level A alerts attributed to the empty channels (solvent accessible voids) and the strong disorder of one of the tta^- anions on two different positions (occupancy probability of 55.6/44.4% and 50.6/49.4% for **1b** and **2**, respectively).

Physical Measurements. Cyclic voltametry was carried out in CH_2Cl_2 solution, containing 0.1 M $^nBu_4NPF_6$ as a supporting electrolyte. Voltamograms were recorded at 100 $mV \cdot s^{-1}$ at a platinum disk electrode. The potentials were measured versus a saturated calomel electrode (SCE; Table 4).

Optical spectra were measured using the KBr disk method on a Perkin-Elmer 1600 Series FT-IR (resolution 4 cm^{-1}) for infrared (IR). Absorption spectra were recorded on a Varian Cary 5000 UV−visible−NIR spectrometer.

The luminescence spectra were measured using a Horiba-JobinYvon Fluorolog-3 spectrofluorimeter, equipped with a three slit double grating excitation and emission monochromator with dispersions of 2.1 nm/mm (1200 grooves/mm).

The dc magnetic susceptibility measurements were performed on solid polycrystalline sample with a Quantum Design MPMS-XL SQUID magnetometer between 2 and 300 K in an applied magnetic field of 0.2 T for temperatures of 2−20 K and 1 T for temperatures of 20−300 K. The experimental data have been corrected from the diamagnetism of the sample holder, and the intrinsic diamagnetism of the materials was evaluated with Pascal's tables.

The hysteresis loop was measured with an Oxford VSM system at a 4 $kOe \cdot min^{-1}$ sweeping rate.

EPR spectra were recorded at 77 K for single crystal $\mathbf{L^{\bullet+}BF_4^-}$ with a BRUKER EMX X-band ESR spectrometer equipped with an OXFORD cryostat. The measures of conductivity were performed on single crystal down to 115 K using the standard two probes method. The difference of potential is measured between two gold wires attached to the crystal with carbon paste.

Computational Details. DFT geometry optimizations and TD-DFT excitation energy calculations of the ligand **L** and Y^{III} dinuclear complex were carried out with the Gaussian 09 (revision A.02) package[17] employing the PBE0 hybrid functional.[18] The "Stuttgart/Dresden" basis sets and effective core potentials were used to describe the yttrium atom,[19] whereas all other atoms were described with the SVP basis sets.[20] The first 50 monoelectronic excitations were calculated for **L**, whereas 100 excitations were necessary for the Y^{III} complex. In all steps, a modeling of bulk solvent effects (solvent = dichloromethane) was included through the Polarizable Continuum Model (PCM),[21] using a linear-response nonequilibrium approach for the TD-DFT step.[22] Molecular orbitals were sketched using the Gabedit graphical interface.[23]

■ RESULTS AND DISCUSSION

Crystal Structure Analysis. We have previously reported the synthesis and crystal structures of the Dy^{III} and Gd^{III} derivatives which were refined at a low temperature (150 K) and room temperature, respectively.[3f] Therein, the X-ray structures of the Eu^{III} (**1**), Nd^{III} (**2**), and Tb^{III} (**3**) derivatives are presented. It is worth noting that only the X-ray structures of the Eu^{III} analogue have been resolved at both low and room temperatures.

$[Eu(tta)_3(L)]_2 \cdot 0.5CH_2Cl_2$ (1a). Compound **1a** crystallizes in the monoclinic $P2_1/n$ (No. 14) space group (Table 1). An ORTEP view is depicted in Figure 1. The structure consists of a centrosymmetric dimetallic unit containing two Eu^{III} ions with a distorted square antiprism. The coordination surrounding is fully oxygenated with eight oxygen atoms arising from three bischelate tta^- anions and two η_2 bridging ligands **L**. The average Eu−O bond length is 2.390(40) Å (Table 2). Using the empirical correlation between the C3−C4 (1.346(11) Å) central bond and C−S (1.758(9) Å) bond lengths of the TTF moieties, the formal charge on the central TTF core is found to be equal to +0.05, which is in agreement with the neutral charge of **L** in **1a**.[24] Neutral complexes **1a** interact through π−π packing (3.244(8)−3.826(9) Å) between one tta^- anion and the TTF core and short S2···O2 contacts (3.151(4) Å; Figure S1) creating channels along the *a* axis (Figures S2 and S3). At

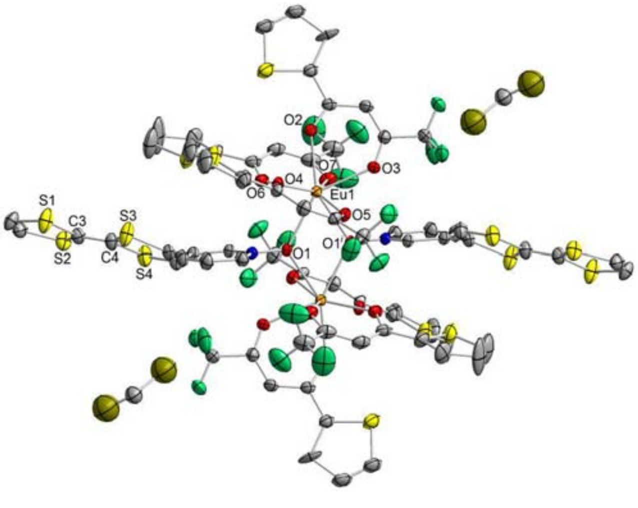

Figure 1. ORTEP view of the dinuclear complex $[Eu(tta)_3(L)]_2 \cdot 0.5CH_2Cl_2$ (**1a**) with labeling scheme. Thermal ellipsoids are drawn at 30% probability. Hydrogen atoms are omitted for clarity.

Table 2. Selected Bond Lengths (Å) and Angles (deg) for Complexes 1−3[a]

compounds	1a	1b	2	3
Ln1−O1	2.443(4)	2.470(4)	2.484(5)	2.419(4)
Ln1−O1^i	2.463(4)	2.447(4)	2.518(5)	2.427(4)
Ln1−O2	2.349(4)	2.353(5)	2.396(5)	2.329(5)
Ln1−O3	2.364(4)	2.405(5)	2.443(5)	2.337(5)
Ln1−O4	2.358(4)	2.356(5)	2.388(5)	2.337(4)
Ln1−O5	2.399(4)	2.363(5)	2.408(5)	2.370(5)
Ln1−O6	2.364(5)	2.347(5)	2.391(5)	2.340(5)
Ln1−O7	2.383(5)	2.385(5)	2.430(5)	2.350(5)
C3−C4	1.346(11)	1.322(13)	1.331(12)	1.339(12)
Ln1−Ln1^i	4.171(1)	4.186(1)	4.250(1)	4.127(1)
ϕ	25.9(2)	24.2(2)	24.5(2)	25.9(2)

[a] ϕ is defined as the torsion angle between the two planes which are formed by the TTF core and the pyridine-*N*-oxide ring.

low temperatures, the channels are filled by the dichloromethane molecules of crystallization. The intramolecular Eu−Eu distance which is equal to 4.171(1) Å is in the same range as those observed in similar systems.[25] The shortest intermolecular Eu−Eu distance is found to be remarkably long with a value of 12.483(5) Å.

[Eu(tta)$_3$(L)]$_2$ (1b). No structural phase transition was observed between 150 and 293 K; thus **1b** crystallizes in the same monoclinic space group as **1a** (Table 1), and the structure of the dinuclear unit at room temperature is the same as that at 150 K (Figure S4). Only the temperature increase has induced the removal of the dichloromethane molecules from the channels (Figures S2 and S3). The intramolecular bond lengths like Eu−O (2.391(5) Å) are not affected by the difference of temperature, while the intermolecular distances increase with the temperature. Thus, the shortest S···O and Eu···Eu distances have been measured equal to 3.288(5) Å and 12.552(7) Å, respectively. The ligand **L** always in its neutral form tends to be more planar at room temperature than at 150 K (see values of the angle ϕ in Table 2).

[Nd(tta)$_3$(L)]$_2$ (2). Compound **2** is isotructural to **1b** (Figure S5). Crystallographic data are given in Tables 1 and 2.

[Tb(tta)$_3$(L)]$_2$·0.5CH$_2$Cl$_2$ (3). Compound **3** is isostructural to **1a** (Tables 1 and 2 and Figure S6). It is worth noting that the X-ray structure of the Tb^{III} derivative could not be refined at room temperature due to the loss of crystallinity of the single crystal. This fact was already observed in the case of the Dy^{III} analogue.[3f] One possible explanation is the smaller ionic radii of Tb^{III} and Dy^{III} compared to the lighter lanthanides, leading to a contraction of the size of the dinuclear unit and consequently an expansion of the channels. If the size of the empty channels is too big compared to the stabilization energy of the intermolecular contacts, the structure falls down, and the crystallinity is lost. That is the case for 4f^n lanthanide derivatives with $n > 7$, while for $n \leq 7$ the X-ray structures can also be obtained without dichloromethane molecules of crystallization. Finally, it can be noticed that the dinuclear complexes cannot be obtained for the smallest ions from Er^{III} to Lu^{III}.

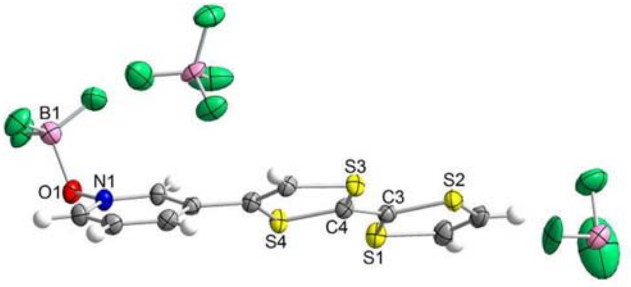

Figure 2. ORTEP view of $\mathbf{L}^{\bullet+}\mathbf{BF}_4^-$. Thermal ellipsoids are drawn at 30% probability.

[L(BF$_3$)]$_2^{\bullet+}$[(BF$_4$)(BF$_3$)]$^-$ ($\mathbf{L}^{\bullet+}\mathbf{BF}_4^-$). Compound $\mathbf{L}^{\bullet+}\mathbf{BF}_4^-$ generated during the electro-crystallization of **2** crystallizes in the orthorhombic *Pnaa* (No. 56) space group (Table 1). An ORTEP view is depicted in Figure 2. The asymmetric unit is composed of one **L**BF$_3$ moiety, a half BF$_3$ molecule, and a half BF$_4^-$ anion. Consequently the charge of the TTF core is +0.5, which is confirmed by the value of the central C3−C4 bond length (1.390(7) Å),[26] larger than under its neutral form in the complexes. The pyridine-*N*-oxide acceptor is coordinated by a molecule of BF$_3$ which comes from the degradation of the BF$_4^-$ anion during the galvanostatic oxidation. Such association between heteroaromatic-*N*-oxide and boron trifluoride is well-known.[27] The B−O bond length of 1.536(8) Å is slightly longer than the distance (1.52 Å) found in classical systems involving a heteroaromatic-*N*-oxide acceptor. This is the consequence of the electronic effect of the coordinated TTF donor. Free BF$_3$ molecules fill the voids of the structure, while the coordinated BF$_3$ interacts with the TTF core as attested by the short C3···B1 (3.649(6) Å) and C4···F3 (2.888(6) Å) distances. The radical cations form dimers along the *b* axis through short S2···S4 (3.431(5) Å) and S1···S3 (3.443(5) Å) contacts that are shorter than the sum of the van der Waals radii (3.65 Å; Figure S7). The shortest S···S distance (4.040(5) Å) between the dimers is longer than the sum of the van der Waals radii.

EPR Measurement and Electronic Conductivity of $\mathbf{L}^{\bullet+}\mathbf{BF}_4^-$. In order to confirm the radical cation form of the ligand, the EPR spectrum of single crystals of $\mathbf{L}^{\bullet+}\mathbf{BF}_4^-$ at 70 K has been obtained (Figure 3a). The spectrum shows a weak and broad signal centered at the isotropic *g* value of 2.0088 (g_1 = 2.0079, g_2 = 2.0155, and g_3 = 2.0029) typical of a radical cation TTF derivative.[28] The intensity of the signal is in agreement with a dimerization of the TTF derivative in the crystal structure of $\mathbf{L}^{\bullet+}\mathbf{BF}_4^-$, leading to radical cations almost completely antiferromagnetically coupled at 70 K.

The electrical resistivity of a single crystal of $\mathbf{L}^{\bullet+}\mathbf{BF}_4^-$ has been measured between 290 and 110 K. Figure 3b shows the temperature dependence of the electrical resistivity of $\mathbf{L}^{\bullet+}\mathbf{BF}_4^-$ at ambient pressure. $\mathbf{L}^{\bullet+}\mathbf{BF}_4^-$ exhibits a semiconducting behavior with a resistivity which increases gradually with decreasing temperature and values of resistivity close to 10 kΩ cm at 110 K.

Electrochemical Properties. The electrochemical properties of **L**, **1**, **2**, and **3** have been studied using cyclic voltametry in a dichloromethane solution (Figure S8). For all compounds, two reversible single-electron-oxidation waves are observed corresponding successively to the formation of the radical cation and dicationic species (Table 3). These values are anodically shifted in comparison with the oxidation potentials measured for the parent TTF (380 and 770 mV) due to the electron-withdrawing nature of the 3-pyridine-*N*-oxide substituent, which makes oxidation of the TTF core more difficult for free ligand **L** and for the coordination complexes **1**, **2**, and **3**. In the case of the complexes, the first oxidation wave remains unchanged, while the second one is anodically shifted in **1**, **2**, and **3** compared to **L**, meaning that the electronic communication should be significant between the TTF core

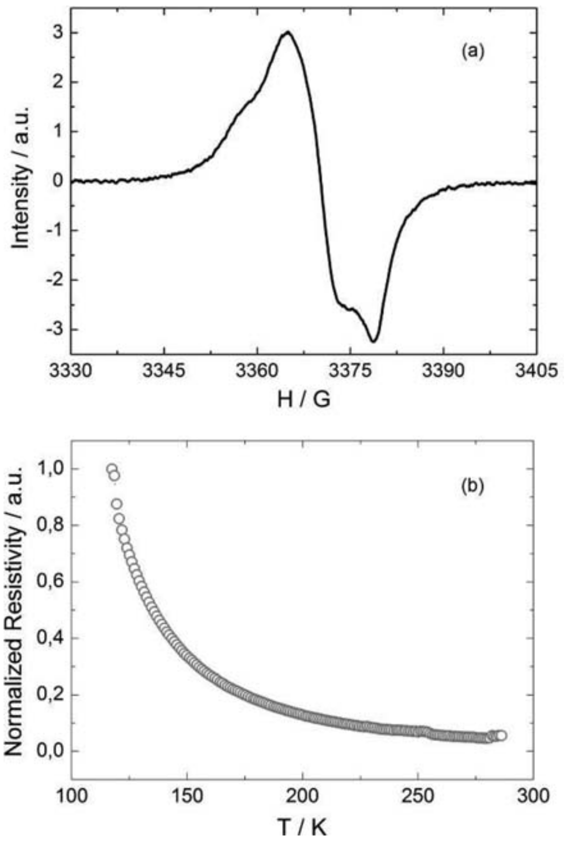

Figure 3. (a) EPR spectrum at 70 K and (b) normalized resistivity in the temperature range 290−110 K of $\mathbf{L}^{\bullet+}\mathbf{BF}_4^{-}$.

Table 3. Oxidation Potentials (V vs. SCE, $^{n}\mathrm{Bu}_4\mathrm{NPF}_6$, 0.1 M in $\mathrm{CH}_2\mathrm{Cl}_2$ at 100 mV·s^{-1}) of Ligand L and Complexes 1−3

	$E_{1/2}{}^{1}$	$E_{1/2}{}^{2}$
L	0.465	0.816
1	0.453	0.867
2	0.460	0.863
3	0.459	0.882

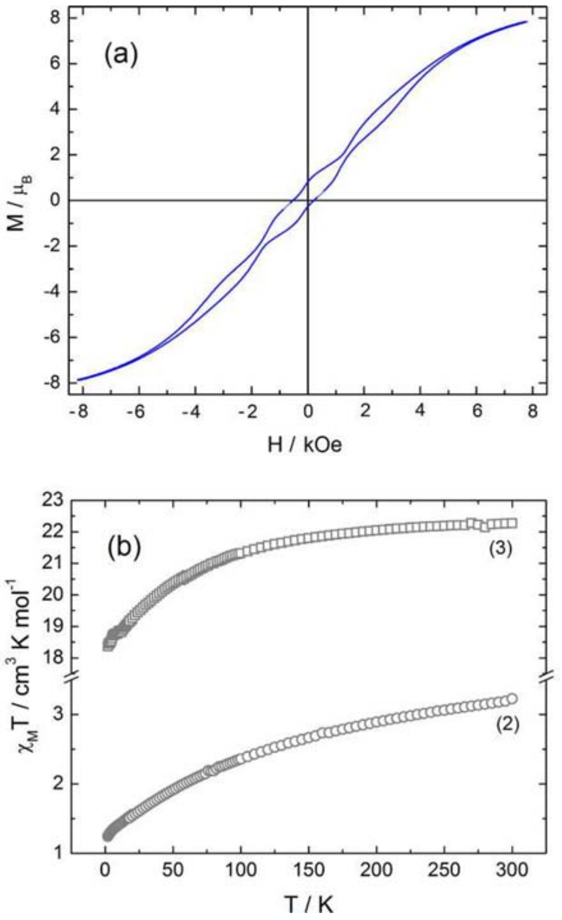

Figure 4. (a) Magnetization vs field loop of $[\mathrm{Dy(tta)}_3(\mathbf{L})]_2\cdot 0.5\mathrm{CH}_2\mathrm{Cl}_2$ (**4**) measured at 1.5 K with a sweep rate of 4 kOe·min^{-1}. (b) Thermal dependence of the $\chi_{\mathrm{M}}T$ product for compounds **2** (gray circles) and **3** (gray squares).

and the Ln$^{\mathrm{III}}$ centers. In fact, the increase of the oxidation potential can be interpreted by the decrease of the electronic density on the TTF core after the coordination of the $\mathrm{Ln(tta)}_3$ fragment. This effect is confirmed by the red shift of the donor−acceptor charge transfer band of the complexes compared to the one for the free ligand (cf. absorption properties).

Magnetic Properties. We have previously demonstrated that the Dy$^{\mathrm{III}}$ analogue displays a SMM behavior with antiferromagnetic interactions between the two Dy$^{\mathrm{III}}$ centers through the *N*-oxide bridges.[3f] Figure 4a depicts its magnetization loop at 1.5 K with a magnetic field sweep rate of 4 kOe·min^{-1}. A "double butterfly" hysteresis is observed. At zero field, the hysteresis is open with a coercive field of 750 Oe. Under applied field, the hysteresis loop is slightly more open (860 Oe at H = 800 Oe) and then narrows (250 Oe at H = 1700 Oe) because of the level crossing between the first excited state and the $m_J = \pm 15/2$ ground state. The H_{crossing} was evaluated to 1300 Oe using an Ising approximation $H_{\mathrm{crossing}} = -J/2g\beta$ with $g = 19.2$ and $J = -2.3$ cm^{-1}. Once the crossing field is overcome, the hysteresis reopens (620 Oe at H = 2800 Oe) to finally close around 10 kOe. Such hysteresis behavior has been observed already for Dy$^{\mathrm{III}}$-based SMMs involving ferro and antiferromagnetic interactions.[29] The thermal dependence of the $\chi_{\mathrm{M}}T$ products for **2** and **3** are shown in Figure 4b and the first magnetization versus the magnetic field in Figure S9. The $\chi_{\mathrm{M}}T(T)$ curves show monotonic decreases from 300 to 2 K. The room temperature values of χ_{M}T are equal to 3.23 cm^3 K mol^{-1} and 22.27 cm^3 K mol^{-1} for **2** and **3**, respectively. These experimental values are in agreement with the expected values of 3.28 cm^3 K mol^{-1} and 23.64 cm^3 K mol^{-1} for two isolated Nd$^{\mathrm{III}}$ ($g_{9/2} = 8/11$) and Tb$^{\mathrm{III}}$ ($g_6 = 3/2$).[30] When the temperature decreases, the $\chi_{\mathrm{M}}T$ (T) curve decreases because of the progressive depopulation of the $J = 9/2$ and $J = 6$ multiplets of the Nd$^{\mathrm{III}}$ and Tb$^{\mathrm{III}}$ even in the absence of any exchange interaction.[31] In the Gd$^{\mathrm{III}}$ and Dy$^{\mathrm{III}}$ analogues, significant antiferromagnetic interactions have been found between the metal centers.[3f] Thus, for compounds **2** and **3**, the decreases are associated with both depopulation and antiferromagnetic interactions. No out-of-phase signal has been observed for the compounds **2** and **3** even under an applied magnetic field. For **3**, a nonsignificant out-of phase signal (less than 5% of the in-phase contribution) is observed at the highest frequencies.

Photophysical Properties. *Absorption Properties.* The experimental absorption properties of the free ligand **L** and the dinuclear complexes **1**−**3** were studied in $\mathrm{CH}_2\mathrm{Cl}_2$ solution (Figures 5a,b and S10). Compound **2** was also studied in the

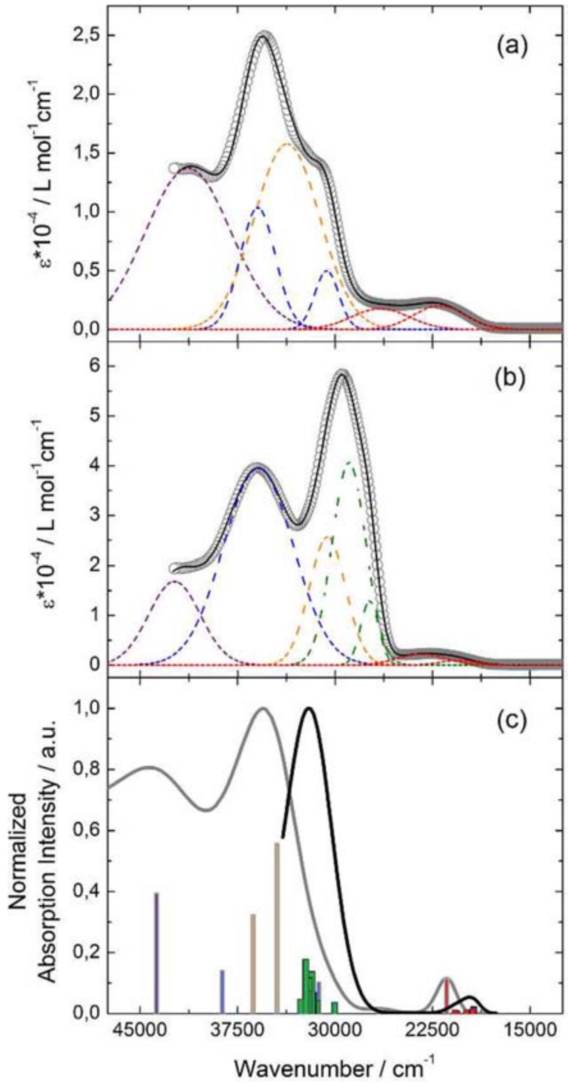

Figure 5. Experimental UV−visible absorption spectra in CH_2Cl_2 solution of compounds **L** (a) and **2** (b) (4×10^{-5} mol L^{-1}) (open gray circles). Respective Gaussian deconvolutions (dashed lines) and best fit (full black line), R = 0.99940 for **L** and R = 0.99993 for **2**. (c) Theoretical absorption spectra of compounds **L** (gray line) and **2** (black line). The fine and large sticks represent the mean contributions of the absorption spectra which are listed in the Table 5 for **L** and **2**, respectively.

solid state to perform a comparison with its emissive properties (Figure 7a). The diamagnetic Y^{III} analogue was considered for DFT calculations (see the Experimental Section). The molecular orbital (MO) diagrams are presented in Figure 6. To support and rationalize the experimental attributions of the absorption data, Time Dependent-Density Functional Theory (TD-DFT) calculations (see the Experimental Section) were performed for **L** and the Y^{III} analogue (Figure 5c and Table 5). The experimental absorption curve of **L** in CH_2Cl_2 solution was deconvoluted in six bands (Figure 5a). The calculated UV−visible absorption spectrum for **L** well reproduces the experimental curve (Figure 5a,c). The lowest energy band was calculated at the value of 21 424 cm^{-1} (experimental value found at 22 000 cm^{-1}, red Gaussian deconvolution) and attributed to π−π* HOMO → LUMO (98%) TTF to 3-Py-*N*-oxide charge transfers (DACT) (Figure 5a, Table 5). The weak absorption band centered at 26 500 cm^{-1} (red deconvolution) was calculated at 26 576 cm^{-1} and attributed to both DACT (HOMO → LUMO+1 (49%)) and intradonor (ID) transition (HOMO → LUMO+2 (47%)). The following absorption band centered at 30 600 cm^{-1} (blue Gaussian deconvolution) was calculated at the energy of 31 253 cm^{-1} and attributed to π−π* intra-acceptor excitation (IA) (HOMO−1 → LUMO (72%)).[32] The strongest absorption band (orange deconvolution) was attributed to ID transition and identified as HOMO → LUMO+4/+7 excitations (Table 5). Finally, the two highest energy absorption bands centered at 35 900 cm^{-1} (blue deconvolution) and 41 300 cm^{-1} (purple deconvolution) were attributed to IA and intraligand (IL) transitions.

The experimental absorption curves of all the dinuclear complexes are very similar (Figures 7 and S10), and so only the one of **2** was discussed. The experimental absorption curve of the dinuclear complex **2** was deconvoluted in seven bands (Figure 5b). An analysis of the molecular orbital diagram shows that the acceptor-centered orbitals are stabilized (0.30 eV) due to the electron withdrawing of the $Ln(tta)_3$ moieties, which decreases the electron density of the acceptor groups (Figure 6) that is weaker than the stabilization observed for the coordination of the $Ln(hfac)_3$ moiety.[3e] The energy of the donor-centered orbitals remains almost unchanged even if the pyridine-*N*-oxide is directly connected to the TTF core (Figure 6). The calculated part well reproduces the experimental absorption curve (Figure 5c). The lowest energy band (20 500 cm^{-1}, red deconvolutions) was identified as surprising ligand to ligand charge transfers (LLCT) from the TTF core to the tta^{-} anions (Figure 5c, Table 5). The expected DACT bands were calculated between 20 635 cm^{-1} and 20 777 cm^{-1} (experimental value is found at 23 400 cm^{-1}) and attributed to the HOMO → LUMO+6 (34%) and HOMO-1 → LUMO+7 (42%) excitations. The coordination of **L** with the $Ln(tta)_3$ precursor leads to a red shift of the DACT band (700 cm^{-1}). The next strong experimental absorption band and its shoulder centered at 27 300 cm^{-1} and 28 900 cm^{-1} (green deconvolutions) were identified as π−π* intratta^{-} (Itta) transitions. It is worth noting that ILCTs from the tta^{-} to the 3-Py-*N*-oxide contribute to this strong absorption band (Table 2). The next orange, blue, and purple absorption deconvolutions were not calculated but nevertheless attributed to ID, IA, and IL transitions by analogy with the calculated absorption bands for the free ligand.

Emission Properties. As previously mentionned, the absorption properties of **2** have also been studied in the solid state (Figure 7a) to be consistent with the emission spectra measured in the solid state, at both room temperature (Figure 7b) and 77 K (Figure 7c and Table S1). Excitation of the free ligand **L** with an energy of 22 200 cm^{-1} at room temperature gives a broad fluorescence band around 670 nm (14 900 cm^{-1}; Figure 7b) and attributed to the CT emission centered on the ligand. It is worth noting that this CT emission has a weak intensity. This behavior is in marked contrast with other TTF-containing ligands that generally exhibit a broad intense emission band.[3c,e,h,33] The emission quenching in the present case could be explained by a Photoinduced Electron Transfer (PET) leading to the formation of the charge separated species in the excited state [$TTF^{\bullet +}$−3-Py-*N*-oxide$^{\bullet -}$]. The recombination leads to luminescence quenching.

Excitation of the neodymium complex **2** in the lowest-energy HOMO→LUMO/+1/+2/+3/+6 and HOMO−1→LUMO/+2/+7 DACTs and LLCT transitions (λ_{ex} = 550−450 nm, 18 200−22 000 cm^{-1}) induces three emission bands in the NIR

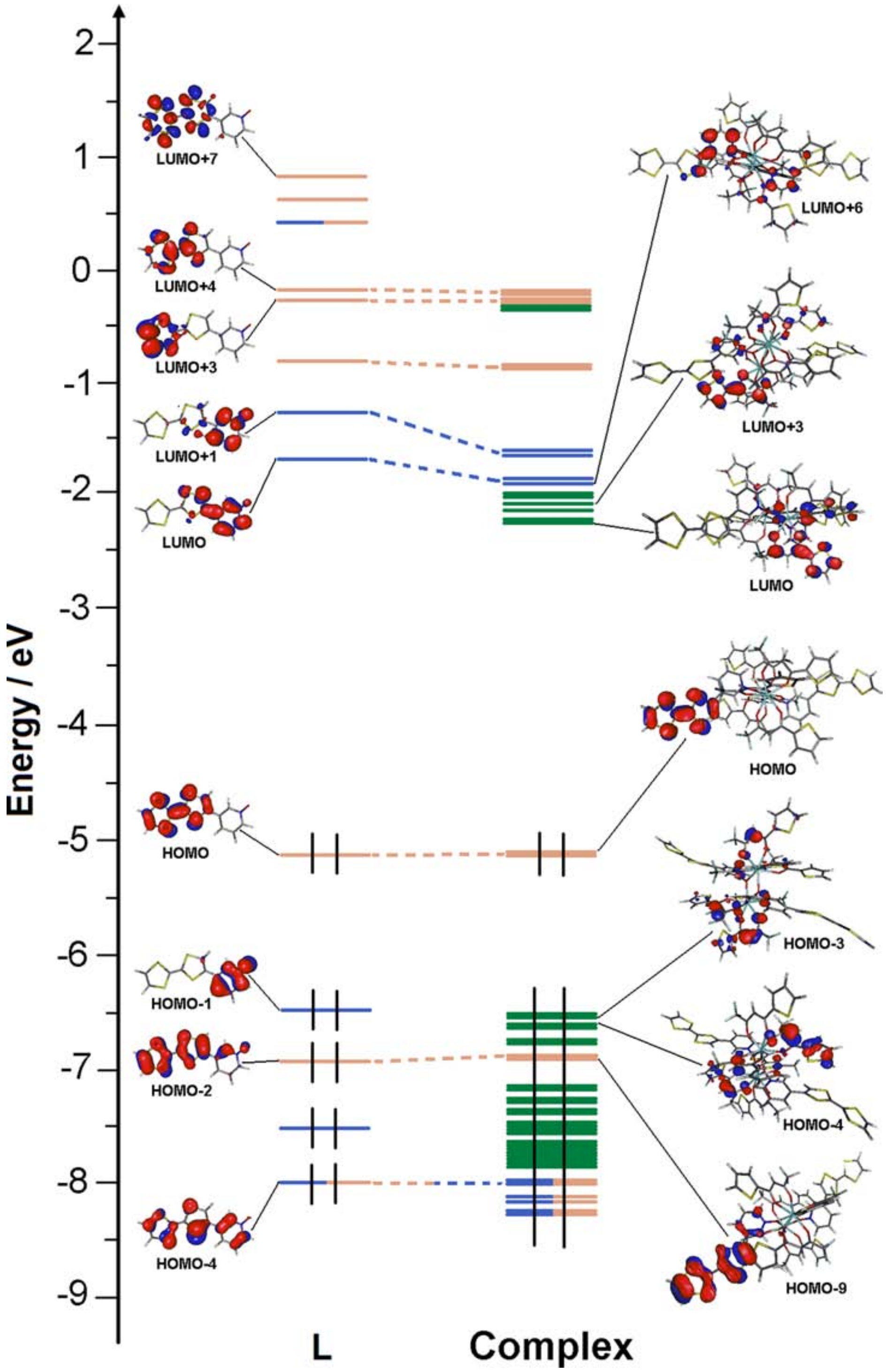

Figure 6. MO diagrams of **L** and $[Y(tta)_3(\mathbf{L})]_2$. Energy levels of the centered TTF donor, 3-Py-*N*-oxide acceptor, and tta$^-$ orbitals are represented in orange, blue, and green color, respectively.

spectral ranges 11 600−10 900, 9500−9100, and 7700−7200 cm^{-1} assigned to the $^4F_{3/2} \rightarrow {}^4I_{9/2}$, $^4F_{3/2} \rightarrow {}^4I_{11/2}$, and $^4F_{3/2} \rightarrow {}^4I_{13/2}$ transitions centered on the neodymium, respectively. The particular excitation at 18 200 cm^{-1} prevents all direct excitations in the weak f−f absorption transitions of the Nd^{III} ion.[34] An additional very weak fluorescence at 685 nm (14 580 cm^{-1}) is observed and attributed to the residual CT emission centered on the ligand (Figure 7b). The energy of the donor excited state can be estimated from the zero-phonon transition wavelength E_{0-0} estimated to 588 nm (17000 cm^{-1}) from the intersection of the absorption and emission spectra. Such excitation wavelength is in the range of the longest wavelengths reported for the Nd sensitization using antenna featuring xanthene (fluoroescein, eosin, erythrosine, or rhodamine 6G, 500−550 nm),[35] bodipy (530 nm),[32,36] or push−pull (550 nm)[37] chromophores but shorter than the wavelength reported for the use of TTF-based radical cation antennae (815 nm).[10,38]

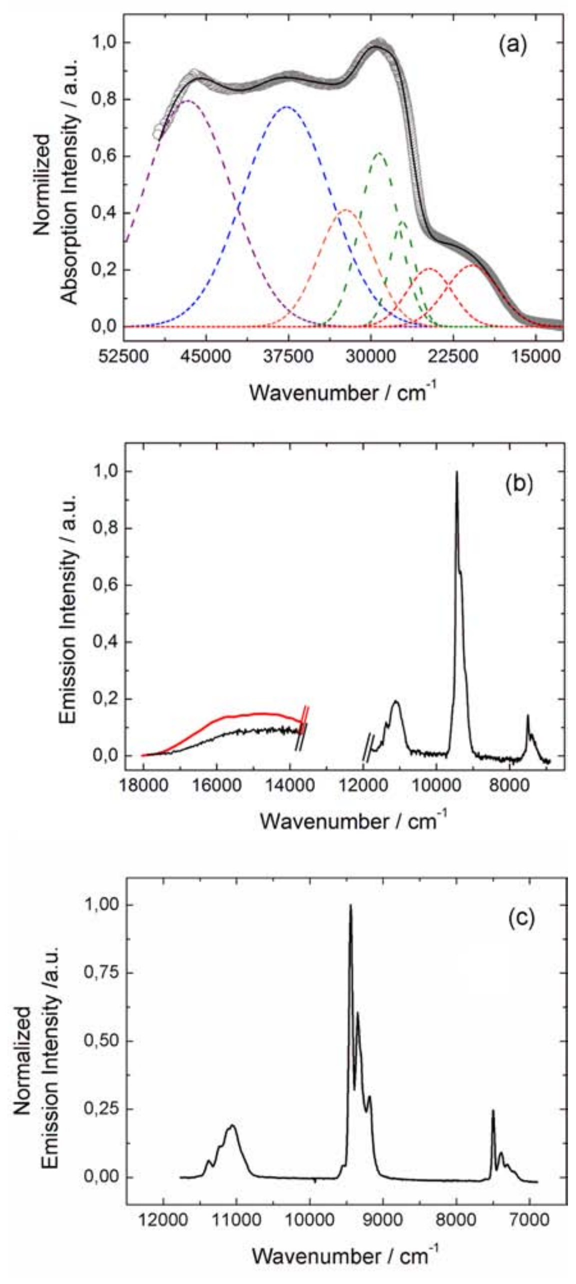

Figure 7. (a) Experimental UV−visible absorption spectrum of **2** in the solid state (KBr pellet; gray open circles). Gaussian deconvolutions are shown as dashed lines and the best fit as a full black line (R = 0.99959). (b) Left part of the figure, emission of free ligand **L** λ_{ex} = 22 200 cm^{-1} (450 nm; red curve) and residual CT emission centered on the ligand for **2** (black curve). On the right part, emission spectra of **2** (black line) in the near-IR for λ_{ex} = 18 200 cm^{-1} (550 nm) in the solid state at room temperature (293 K). (c) Emission spectra of **2** (black line) in the near-IR for λ_{ex} = 18 200 cm^{-1} (550 nm) in the solid state at 77 K.

Cooling down the solid at 77 K gives a far better resolved luminescence spectrum (Figure 7c), and the clear splitting of each transition is observed; the $^4F_{3/2}\rightarrow^4I_{9/2}$, $^4F_{3/2}\rightarrow^4I_{11/2}$, and $^4F_{3/2}\rightarrow^4I_{13/2}$ present 5, 4, and 4 main components, respectively (Figure S11). It is well-known that such splitting is correlated to the ligand- (crystal-) field effect and consequently is a signature of the local symmetry. For a Nd ion low site symmetry (typically here in a D_{4d} symmetric environment), a theoretical splitting of 5, 6, and 7 is expected.[34] Experimentally, only the higher energy transition shows the expected splitting; in the other emission bands, spectral overlap at 77 K explains the lower splitting observation.

Table 4. Absorption Data for the Ligand L and Complexes 1−3

	L in CH_2Cl_2 solution	**1** in CH_2Cl_2 solution	**2** in solid state	**2** in CH_2Cl_2 solution	**3** in CH_2Cl_2 solution
experimental energies (cm^{-1})	22000	20500	20800	20500	21000
	26500	23400	24700	23400	23900
	30600	27400	27200	27300	27300
	33700	29100	29300	28900	28800
	35900	30700	32300	30600	30600
	41300	35900	37700	35900	35900
		42200	46700	42400	42400

In the literature, TTF-containing antenna are generally involved in two types of sensitization processes: (i) An energy transfer pathway from the lowest energy charge transfer excited state is generally encountered in the cases of Nd^{III} or Er^{III} derivatives. (ii) A stepwise electron transfer mechanism involving transient Yb^{II} species must be considered in the case of Yb^{III} derivatives. In the present case, complex **2** exhibits a low energy CT transition centered on the TTF containing antennae, and consequently a classical energy transfer mechanism can be envisaged. Nevertheless, the redox activity of **L** and **2** at modest potential, combined with the isolation of **L**$^{\bullet+}$ radical cation and the possible emission quenching for **L** due to the PET process, prompt us to propose an alternative sensitization pathway. By analogy with the famous anthracene substituted 2-(2-pyridyl)benzimidazole ligand reported by Ward et al.,[39] this sensitization pathway may involve the transient formation of an oxidized donor/reduced acceptor [TTF$^{\bullet+}$−3-Py-*N*-oxide$^{\bullet-}${Nd(tta)$_3$}] species that will generate the emissive Nd^{III} excited state after back electron transfer. According to the above-mentioned studies,[3a,b,9e] it is possible to estimate the feasibility of the photoinduced electron transfer (ΔG_{ET}) using the following extended Rehm−Weller[40] equation:

$$\Delta G_{ET} \geq e_0(E_{ox} - E_{red}) - E_{0-0} - w$$

where e_0 represents the elementary electron charge; E_{ox}, the oxidation potential of the electro-donating ligand; E_{red}, the reduction potential of the acceptor; and E_{0-0} the excited state energy. In addition, w represents the stabilization energy between the different components of the ion pair (0.15 eV for a closely associated ion pair). On one hand, cyclic voltametry revealed an irreversible reduction, assumed to be 3-Py-*N*-oxide centered at −1.55 V (value determined from the free ligand **L**) and a reversible oxidation at 0.460 V vs SCE (value determined from the complex **2**). The energy of the excited state corresponding to the zero phonon transition is estimated to E_{0-0} = 2.109 eV and the equation becomes $\Delta G_{ET} \geq 1 \times (0.460 + 1.55) - 2.109 - 0.15$; hence, $\Delta G_{ET} \geq -0.249$ eV. The negative value of ΔG_{ET} confirms the feasibility of a photoinduced electron transfer. In addition, since the reduction of the 3-Py-*N*-oxide unit becomes much easier when the ligand is coordinated to an electropositive metal center,[41] E_{red} becomes more negative. Within this approximation, the Rehm−Weller equation gives a negative ΔG_{ET} value for **2**, suggesting a mechanism involving a thermodynamically favored ligand centered electron transfer process via the formation of

Table 5. TD-DFT Calculated Excitation Energies and Main Compositions of the Low-Lying Electronic Transitions for L, and Y^{III} Derivative[a]

	E exp (cm^{-1})	E theo (cm^{-1})	osc.	type	assignment	transition
L	22000	21424	0.09	DACT	$\pi_{\text{TTF}}\rightarrow\pi^{*}_{\text{Py-N-oxide}}$	H→L (97%)
	26500	26576	0.01	DACT+ ID	$\pi_{\text{TTF}}\rightarrow\pi^{*}_{\text{Py-N-oxide}} + \pi_{\text{TTF}}\rightarrow\pi^{*}_{\text{TTF}}$	H→L+1 (49%) H→L+2 (47%)
	30600	31253	0.08	IA	$\pi_{\text{Py-N-oxide}}\rightarrow\pi^{*}_{\text{Py-N-oxide}}$	H-1→L (72%)
	33700	34473	0.44	ID	$\pi_{\text{TTF}}\rightarrow\pi^{*}_{\text{TTF}} + \pi_{\text{TTF}}\rightarrow\sigma^{*}_{\text{TTF}}$	H→L+4 (58%)
		36320	0.26			H→L+7 (49%) H→L+4 (27%)
	35900	38685	0.11	IA	$\pi_{\text{Py-N-oxide}}\rightarrow\pi^{*}_{\text{Py-N-oxide}}$	H-1→L+1 (43%)
	41300	43743	0.31	IL	$\pi_{\text{L}}\rightarrow\pi^{*}_{\text{L}}$	H-4→L (69%)
2	20500/20800[b]	19332	0.08	LLCT	$\pi_{\text{TTF}}\rightarrow\pi^{*}_{\text{tta}}$	H-1→L/+2 (25/51%)
		19455	0.05			H→L+2/+3 (30/52%)
		19893	0.04			H→L/+1 (53/18%)
	23400/24700[b]	20635	0.03	DACT	$\pi_{\text{TTF}}\rightarrow\pi^{*}_{\text{Py-N-oxide}}$	H→L+6 (34%)
		20777	0.04			H-1→L+7 (42%)
	27300/27200[b]	30046	0.13	Itta	$\pi_{\text{tta}}\rightarrow\pi^{*}_{\text{tta}}$	H-3→L+2 (57%)
	28900/29300[b]	31781	0.35	Itta + LLCT	$\pi_{\text{tta}}\rightarrow\pi^{*}_{\text{tta}} + \pi_{\text{tta}}\rightarrow\pi^{*}_{\text{Py-N-oxide}}$	H-5→L+2 (20%) H-4→L+4 (16%)
		31990	0.25			H-7→L+2 (11%) H-3→L+6 (16%)
		32276	0.29			H-5→L+3 (10%) H-4→L+6 (20%)
	30600/32300[b]			ID	$\pi_{\text{TTF}}\rightarrow\pi^{*}_{\text{TTF}}$	
	35900/37700[b]			IA	$\pi_{\text{Py-N-oxide}}\rightarrow\pi^{*}_{\text{Py-N-oxide}}$	
	42400/46700[b]			IL	$\pi_{\text{L}}\rightarrow\pi^{*}_{\text{Py-N-oxide}}$	

[a] In addition, the charge transfer and the pure intramolecular transitions are reported. ID, IA, IL, Itta^{-} and H, L, nb represent the intramolecular TTF (donor), 3-py-*N*-oxide (acceptor), whole ligand, tta^{-} transitions, the HOMO, and the LUMO, respectively. Therefore, LLCT stands for ligand to ligand charge transfer and DACT for donor−acceptor charge transfer. The theoretical values are evaluated at the PCM(CH_2Cl_2)-PBE0/SVP level of approximation. [b] Experimental values obtained from the Gaussian deconvolutions of the solid-state absorption spectrum.

separated charge excited state [$TTF^{\bullet+}$−3-Py-*N*-oxide$^{\bullet-}${Nd-$(tta)_3$}] by analogy with the above-mentioned anthracene case. Upon charge recombination, the emissive [TTF−3-Py-*N*-oxide{Nd*$(tta)_3$}] species may be generated. Attempts to observe the formation of the radical cation and anion by EPR measurements under photoirradiation (24750 cm^{-1}) were undertaken without success. Transient absorption measurements could be a better technique to directly observe the formation of such charge-separated state.[39d]

CONCLUSIONS

Three centro-symmetric dinuclear complexes of Eu^{III} (**1**), Nd^{III} (**2**), and Tb^{III} (**3**) involving the tetrathiafulvalene-3-py-*N*-oxide ligand have been studied. For **1**, the X-ray structure could be solved with the filled (**1a**) and empty channels (**1b**). It has been established that for the big $4f^{n}$ lanthanide ions (with $n \leq 7$), the X-ray structures can be obtained with and without dichloromethane molecules of crystallization, while for $n > 7$, the size of the empty channels is too big to support the loss of the solvent, and the structure falls down.

Thermal electronic conductivity has revealed semiconductor behavior for the $\mathbf{L^{\bullet+}BF_4^{-}}$ radical cation. The Dy^{III} analogue has shown a complex butterfly like hysteresis loop at 1.5 K. This observation corroborates the SMM behavior of this derivative.

Irradiation at 22 200 cm^{-1} of the lowest-energy HOMO→LUMO charge transfer band of **L** leads to a weak and broad fluorescence band. Actually the irradiation of **2** (18 200−22 000 cm^{-1}) at 77 K and room temperature reveals only the classical Nd^{III} centered luminescence assigned to the $^4F_{3/2}\rightarrow$ $^4I_{9/2}$, $^4F_{3/2}\rightarrow$ $^4I_{11/2}$, and $^4F_{3/2}\rightarrow$ $^4I_{13/2}$ transitions. The sensitization mechanism of the Nd^{III} luminescence can proceed via a classical CT excited state of the antenna or via an unusual ligand centered photoinduced electron transfer. The possibility of this ligand **L** to generate the separated-charge state opens new perspectives for this series of complexes such as photoinduced electronic conductivity and thus the feasibility of obtaining switchable photoinduced conducting single molecule magnets. The irradiation effects on the single molecule magnet behavior of the Dy^{III} analogue are in progress in our group.

ASSOCIATED CONTENT

Ⓢ Supporting Information

Crystallographic information in CIF format, ORTEP views for **1b**, **2**, and **3** (Figures S4−S6); packing views (Figures S2, S3, and S7); cyclic voltametry for **1**, **2**, and **3** (Figure S8); M(H) curves for **2** and **3** (Figure S9); UV−visible absorption spectra for **1** and **3** (Figure S10); Gaussian deconvolution of the emission spectra of **2** (Figure S11); and crystal-field sublevels of the Nd(^4I_J) (Table S1). This material is available free of charge via the Internet at http://pubs.acs.org.

AUTHOR INFORMATION

Corresponding Author

*E-mail: fabrice.pointillart@univ-rennes1.fr.

Notes

The authors declare no competing financial interest.

ACKNOWLEDGMENTS

This work was supported by the CNRS, Rennes Métropole, Université de Rennes 1, Région Bretagne and FEDER.

■ REFERENCES

(1) Coleman, L. B.; Cohen, M. J.; Sandman, D. J.; Yamagashi, F. G.; Gitaro, A. F.; Ferraris, A. F. *Solid State Commun.* **1973**, *12*, 1125.

(2) (a) Lorcy, D.; Bellec, N.; Fourmigué, M.; Avarvari, N. *Coord. Chem. Rev.* **2009**, *253*, 1398 and references therein. (b) Fourmigué, M.; Ouahab, L. *Conducting and Magnetic Organometallic Molecular Materials*; Springer: New York, 2009. (c) Ouahab, L.; Enoki, T. *Eur. J. Inorg. Chem.* **2004**, 933. (d) Kobayashi, H.; Kobayashi, A.; Cassoux, P. *Chem. Soc. Rev.* **2000**, *29*, 325. (e) Kobayashi, A.; Fijiwara, E.; Kobayashi, H. *Chem. Rev.* **2004**, *104*, 5243. (f) Kurmoo, M.; Graham, A. W.; Day, P.; Coles, S. J.; Hurtsthouse, M. B.; Caufield, J. M.; Singleton, J.; Ducasse, L.; Guionneau, P. *J. Am. Chem. Soc.* **1995**, *117*, 12209. (g) Coronado, E.; Day, P. *Chem. Rev.* **2004**, *104*, 5419. (h) Ojima, E.; Fujiwara, H.; Kato, K.; Kobayashi, H.; Tanaka, H.; Kobayashi, A.; Tokumoto, M.; Cassoux, P. *J. Am. Chem. Soc.* **1999**, *121*, 5581 and references therein. (i) Tanaka, H.; Kobayashi, H.; Kobayashi, A.; Cassoux, P. *Adv. Mater.* **2000**, *12*, 1685. (b) Uji, S.; Shinagawa, H.; Terashima, T.; Terakura, C.; Yakabe, T.; Terai, Y.; Tokumoto, M.; Kobayashi, A.; Tanaka, H.; Kobayashi, H. *Nature* **2001**, *410*, 908.

(3) (a) Faulkner, S.; Burton-Pye, B. P.; Khan, T.; Martin, L. R.; Wray, S. D.; Skabara, P. J. *Chem. Commun.* **2002**, *16*, 1668. (b) Pope, S. J. A.; Burton-Pye, P. B.; Berridge, R.; Khan, T.; Skabara, P.; Faulkner, S. *Dalton Trans.* **2006**, 2907. (c) Pointillart, F.; Le Gal, Y.; Golhen, S.; Cador, O.; Ouahab, L. *Inorg. Chem.* **2009**, *48*, 4631. (d) Pointillart, F.; Le Gal, Y.; Golhen, S.; Cador, O.; Ouahab, L. *Chem. Commun.* **2009**, 3777. (e) Pointillart, F.; Cauchy, T.; Maury, O.; Le Gal, Y.; Golhen, S.; Cador, O.; Ouahab, L. *Chem.—Eur. J.* **2010**, *16*, 11926. (f) Pointillart, F.; Le Gal, Y.; Golhen, S.; Cador, O.; Ouahab, L. *Chem.—Eur. J.* **2011**, *17*, 10397. (g) Cosquer, G.; Pointillart, F.; Le Gal, Y.; Golhen, S.; Cador, O.; Ouahab, L. *Chem.—Eur. J.* **2011**, *17*, 12502. (h) Pointillart, F.; Bourdolle, A.; Cauchy, T.; Maury, O.; Le Gal, Y.; Golhen, S.; Cador, O.; Ouahab, L. *Inorg. Chem.* **2012**, *51*, 978. (i) Pointillart, F.; Klementieva, S.; Kuropatov, V.; Le Gal, Y.; Golhen, S.; Cador, O.; Cherkasov, V.; Ouahab, L. *Chem. Commun* **2012**, *48*, 714. (j) Ran, Y.-F.; Steinmann, M.; Sigrist, M.; Liu, S.-X.; Hauser, J.; Decurtins, S. *C. R. Chim.* **2012**, *15*, 838.

(4) (a) Sessoli, R.; Tsai, H. L.; Schake, A. R.; Wang, S. Y.; Vincent, J. B.; Folting, K.; Gatteschi, D.; Christou, G.; Hendrickson, D. N. *J. Am. Chem. Soc.* **1993**, *115*, 1804. (b) Sessoli, R.; Gatteschi, D.; Caneschi, A.; Novak, M. A. *Nature* **1993**, *365*, 141. (c) Gatteschi, D.; Sessoli, R.; Villain, J. *Molecular Nanomagnets*; Oxford University Press: New York, 2006. (d) Gatteschi, D.; Sessoli, R. *Angew. Chem., Int. Ed.* **2003**, *42*, 268.

(5) (a) Yamanouchi, M.; Chiba, D.; Matsukura, F.; Ohno, H. *Nature* **2004**, *428*, 532. (b) Saitoh, E.; Miyajima, H.; Yamaoka, T.; Tatara, G. *Nature* **2004**, *432*, 203. (c) Evangelisti, M.; Luis, F.; De Jongh, L. J.; Affronte, M. *J. Mater. Chem.* **2006**, *16*, 2534. (d) Manoli, M.; Collins, A.; Parsons, S.; Candini, A.; Evangelisti, M.; Brechin, E. K. *J. Am. Chem. Soc.* **2008**, *130*, 11129. (e) Bogani, L.; Wernsdorfer, W. *Nat. Mater.* **2008**, *7*, 179. (f) Leuenberger, M. N.; Loss, D. *Nature* **2001**, *410*, 789.

(6) Guo, Y.-N.; Xu, G.-F.; Guo, Y.; Tang, J. *Dalton Trans.* **2011**, *40*, 9953 and references therein.

(7) Katoh, K.; Isshiki, H.; Komeda, T.; Yamashita, M. *Coord. Chem. Rev.* **2011**, *255*, 2124 and references therein.

(8) (a) Sabbatini, N.; Guardigli, M.; Manet, I. *Handbook of the Physics and Chemistry of Rare Earths*; Elsevier: Amsterdam, 1996; Vol. *23*, p 69. (b) Comby, S.; Bünzli, J.-C. G. *Handbook on the Physics and Chemistry of Rare Earths*; Elsevier BV: Amsterdam, 2007; Chapter 235, Vol. 37.

(9) (a) Parker, D. *Coord. Chem. Rev.* **2000**, *205*, 109. (b) Parker, D. *Chem. Soc. Rev.* **2004**, *33*, 156. (c) Bünzli, J.-C. G.; Piguet, C. *Coord. Chem. Rev.* **2005**, *34*, 1048. (d) Eliseeva, S. V.; Bünzli, J.-C. G. *Coord. Chem. Rev.* **2010**, *39*, 189 and references therein. (e) D'Aléo, A.; Pointillart, F.; Ouahab, L.; Andraud, C.; Maury, O. *Coord. Chem. Rev.* **2012**, *256*, 1604 and references therein. (f) D'Aleo, A.; Picot, P.; Beeby, A.; Williams, J. A. G.; Le Guennic, B.; Andraud, C.; Maury, O. *Inorg. Chem.* **2008**, *47*, 10258. (g) Yang, C.; Fu, L.-M.; Wang, Y.; Zhang, J.-P.; Wong, W.-T.; Ai, X.-C.; Qiao, Y.-F.; Zou, B.-S.; Gui, L.-L. *Angew. Chem., Int. Ed.* **2004**, *43*, 5010.

(10) Pointillart, F.; Maury, O.; Le Gal, Y.; Golhen, S.; Cador, O.; Ouahab, L. *Inorg. Chem.* **2009**, *48*, 7421.

(11) (a) Faulkner, S.; Matthews, J. L. Fluorescent complexes for biomedical applications. In *Comprehensive Coordination Chemistry*, 2nd ed.; Ward, M. D., Ed.; Elsevier: New York, 2004; Vol. *9*, 913. (b) Motson, G. R.; Fleming, J. S. *Adv. Inorg. Chem.* **2004**, *55*, 361. (c) Zang, F. X.; Hong, Z. R.; Li, W. L.; Li, M. T.; Sun, X. Y. *Appl. Phys. Lett.* **2004**, *84*, 2679. (d) Suzuki, H. *J. Photochem. Photobiol., A* **2004**, *166*, 155. (e) Tanabe, S. *C. R. Chim.* **2002**, *5*, 815.

(12) (a) Comby, S.; Bünzli, J.-C. G. In *Handbook on the Physics and Chemistry of rare Earths*; Karl, J.; Gschneidner, A.; Bünzli, J.-C. G.; Pecharsky, V. K., Ed.; Elsevier: New York, 2007; Vol. *37*, p 217. (b) Bünzli, J.-C. G. *Chem. Rev.* **2010**, *110*, 2729.

(13) Fujiwara, H.; Yokota, S.; Hayashi, S.; Takemoto, S.; Matsuzaka, H. *Physica B* **2010**, *405*, S15.

(14) (a) Bryce, M. R. *Adv. Mater.* **1999**, *11*, 11. (b) Nishikawa, H.; Kojima, S.; Kodama, T.; Ikemoto, I.; Suzuki, S.; Kikuchi, K.; Fujitsuka, M.; Luo, H.; Araki, Y.; Ito, O. *J. Phys. Chem. A* **2004**, *108*, 1881.

(15) Vooshin, A. I.; Shavaleev, N. M.; Kazakov, V. P. *J. Lumin.* **2000**, *91*, 49.

(16) Sheldrick, G. M. *SHELX97*, release 97-2; Institüt für Anorganische Chemie der Universität: Göttingen, Germany, 1998. *SIR97*: Altomare, A.; Burla, M. C.; Camalli, M.; Cascarano, G. L.; Giacovazzo, C.; Guagliardi, A.; Moliterni, A. G. G.; Polidori, G.; Spagna, R. *J. Appl. Crystallogr.* **1999**, *32*, 115.

(17) Frisch, M. J.; Trucks, G. W.; Schlegel, H. B.; Scuseria, G. E.; Robb, M. A.; Cheeseman, J. R.; Scalmani, G.; Barone, V.; Mennucci, B.; Petersson, G. A.; Nakatsuji, H.; Caricato, M.; Li, X.; Hratchian, H. P.; Izmaylov, A. F.; Bloino, J.; Zheng, G.; Sonnenberg, J. L.; Hada, M.; Ehara, M.; Toyota, K.; Fukuda, R.; Hasegawa, J.; Ishida, M.; Nakajima, T.; Honda, Y.; Kitao, O.; Nakai, H.; Vreven, T.; Montgomery, J. A., Jr.; Peralta, J. E.; Ogliaro, F.; Bearpark, M.; Heyd, J. J.; Brothers, E.; Kudin, K. N.; Staroverov, V. N.; Kobayashi, R.; Normand, J.; Raghavachari, K.; Rendell, A.; Burant, J. C.; Iyengar, S. S.; Tomasi, J.; Cossi, M.; Rega, N.; Millam, J. M.; Klene, M.; Knox, J. E.; Cross, J. B.; Bakken, V.; Adamo, C.; Jaramillo, J.; Gomperts, R.; Stratmann, R. E.; Yazyev, O.; Austin, A. J.; Cammi, R.; Pomelli, C.; Ochterski, J. W.; Martin, R. L.; Morokuma, K.; Zakrzewski, V. G.; Voth, G. A.; Salvador, P.; Dannenberg, J. J.; Dapprich, S.; Daniels, A. D.; Farkas, O.; Foresman, J. B.; Ortiz, J. V.; Cioslowski, J.; Fox, D. J. *Gaussian 09*, revision A.02; Gaussian Inc.: Wallingford, CT, 2009.

(18) (a) Adamo, C.; Barone, V. *J. Chem. Phys.* **1999**, *110*, 6158. (b) Ernzerhof, M.; Scuseria, G. E. *J. Chem. Phys.* **1999**, *110*, 5029.

(19) Dolg, M.; Stoll, H.; Preuss, H. *Theor. Chem. Acc.* **1993**, *85*, 441.

(20) Weigend, F.; Ahlrichs, R. *Phys. Chem. Chem. Phys.* **2005**, *7*, 3297.

(21) Tomasi, J.; Mennucci, B.; Cammi, R. *Chem. Rev.* **2005**, *105*, 2999.

(22) (a) Cossi, M.; Barone, V. *J. Chem. Phys.* **2001**, *115*, 4708. (b) Improta, R.; Barone, V.; Scalmani, G.; Frisch, M. J. *J. Chem. Phys.* **2006**, *125*, 054103.

(23) Allouche, A.-R. *J. Comput. Chem.* **2011**, *32*, 174.

(24) (a) Umland, T. C.; Allie, S.; Kuhlmann, T.; Coppens, P. *J. Phys. Chem.* **1988**, *92*, 6456. (b) Wang, L.; Zhang, B.; Zhang, J. *Inorg. Chem.* **2006**, *45*, 6860. (c) Iwahori, F.; Golhen, S.; Ouahab, L.; Carlier, R.; Sutter, J. P. *Inorg. Chem.* **2001**, *40*, 6541. (d) Cosquer, G.; Pointillart, F.; Le Gal, Y.; Golhen, S.; Cador, O.; Ouahab, L. *Dalton Trans.* **2009**, 3495.

(25) Eliseeva, S. V.; Ryazanov, M.; Gumy, F.; Troyanov, S. I.; Lepnev, L. S.; Bünzli, J.-C. G.; Kuzmina, N. P. *Eur. J. Inorg. Chem.* **2006**, 4809.

(26) Setifi, F.; Ouahab, L.; Golhen, S.; Yoshida, Y.; Saito, G. *Inorg. Chem.* **2003**, *42*, 1791.

(27) Nizhnik, Y. P.; Lu, J.; Rosokha, S. V.; Kochiz, J. K. *New J. Chem.* **2009**, *33*, 2317.

(28) Scout, J. S. In *Highly Conducting Quasi-One-Dimensional Organic Crystals*; Conswell, E., Ed.; Academic Press: New York, 1988; Semiconductors and Semimetals, Vol. 27, p 385.

(29) (a) Guo, Y.-N.; Xu, G.-F.; Wernsdorfer, W.; Ungur, L.; Guo, Y.; Tang, J.; Zhang, H.-J.; Chibotaru, L. F.; Powell, A. K. *J. Am. Chem. Soc.* **2011**, *133*, 11948. (b) Tian, H.; Wang, M.; Zhao, L.; Guo, Y.-N.; Guo, Y.; Tang, J.; Liu, Z. *Chem.—Eur. J.* **2012**, *18*, 442. (c) Meihaus, K. R.; Rinehart, J. D.; Long, J. R. *Inorg. Chem.* **2011**, *50*, 8484. (d) Costes, J. P.; Dahan, F.; Dupuis, A.; Laurent, J. P. *Chem.—Eur. J.* **1998**, *4*, 1616. (e) Katoh, K.; Kajiwara, T.; Nakano, M.; Nakazawa, Y.; Wernsdorfer, W.; Ishikawa, N.; Breedlove, B. K.; Yamashita, M. *Chem.—Eur. J.* **2011**, *17*, 117. (f) Xu, G. F.; Wang, Q. L.; Gamez, P.; Ma, Y.; Clerac, R.; Tang, J. K.; Yan, S. P.; Cheng, P.; Liao, D. Z. *Chem. Commun.* **2010**, *46*, 1506. (g) Lin, P. H.; Burchell, T. J.; Ungur, L.; Chibotaru, L. F.; Wernsdorfer, W.; Murugesu, M. *Angew. Chem., Int. Ed.* **2009**, *48*, 9489. (h) Long, J.; Habib, F.; Lin, P. H.; Korobkov, I.; Enright, G.; Ungur, L.; Wernsdorfer, W.; Chibotaru, L. F.; Murugesu, M. *J. Am. Chem. Soc.* **2011**, *133*, 5319. (i) Layfield, R. A.; McDouall, J. J. W.; Sulway, S. A.; Tuna, F.; Collison, D.; Winpenny, R. E. P. *Chem.—Eur. J.* **2010**, *16*, 4442.

(30) Kahn, O. *Molecular Magnetism*; Wiley-VCH: New York, 1993.

(31) Rinehart, J. D.; Long, J. R. *Chem. Sci.* **2011**, *2*, 2078.

(32) Pointillart, F.; Cauchy, T.; Le Gal, Y.; Golhen, S.; Cador, O.; Ouahab, L. *Inorg. Chem.* **2010**, *49*, 1947.

(33) (a) Jia, C.; Liu, S.-X.; Tanner, C.; Leiggener, C.; Neels, A.; Sanguinet, L.; Levillain, E.; Leutwyler, S.; Hauser, A.; Decurtins, S. *Chem.—Eur. J.* **2007**, *13*, 3804. (b) Goze, C.; Dupont, N.; Beitler, E.; Leiggener, C.; Jia, H.; Monbaron, P.; Liu, S.-X.; Neels, A.; Hauser, A.; Decurtins, S. *Inorg. Chem.* **2008**, *47*, 11010.

(34) Ziessel, R. F.; Ulrich, G.; Charbonnière, L.; Imbert, D.; Scopelliti, R.; Bünzli, J.-C. G. *Chem.—Eur. J.* **2006**, *12*, 5060.

(35) Mech, A. *Polyhedron* **2008**, *27*, 393.

(36) (a) Huang, W.; Wu, D.; Guo, D.; Zhu, X.; He, C.; Meng, Q.; Duan, C. *Dalton Trans.* **2009**, 2081. (b) Hebbink, G. A.; Grave, L.; Woldering, L. A.; Reinhoudt, D. N.; van Veggel, F. C. J. M. *J. Phys. Chem. A.* **2003**, *107*, 2483. (c) Werts, M. H. V.; Hofstraat, J. W.; Geurts, F. A. J.; Verhoeven, J. W. *Chem. Phys. Lett.* **1997**, *276*, 196. Albrecht, M.; Osetska, O.; Klankermayer, J.; Fröhlich, R.; Gumy, F.; Bünzli, J.-C. G. *Chem. Commun.* **2007**, 1834. Shavaleev, N. M.; Scopelliti, R.; Gumy, F.; Bünzli, J.-C. G. *Inorg. Chem.* **2009**, *48*, 2908.

(37) (a) Zhong, Y.; Si, L.; He, H.; Sykes, A. G. *Dalton Trans.* **2011**, *40*, 11389. (b) He, H.; Si, L.; Zhong, Y.; Dubey, M. *Chem. Commun.* **2012**, *48*, 1886.

(38) (a) Shavaleev, N. M.; Scopelliti, R.; Gumy, F.; Bünzli, J.-C. G. *Eur. J. Inorg. Chem.* **2008**, 1523. (b) Baek, N. S.; Kim, Y. H.; Eom, Y. K.; Oh, J. H.; Kim, H. K.; Aebischer, A.; Gumy, F.; Chauvin, A.-S.; Bünzli, J.-C. G. *Dalton Trans.* **2010**, *39*, 1532.

(39) (a) Horrocks De, W. W., Jr.; Bolender, J. P.; Smith, W. D.; Supkowski, R. M. *J. Am. Chem. Soc.* **1997**, *119*, 5972. (b) Supkowski, R. M.; Bolender, J. P.; Smith, W. D.; Reynolds, L. E. L.; Horrocks De, W. W., Jr. *Coord. Chem. Rev.* **1999**, *185−186*, 307. (c) Beeby, A.; Faulkner, S.; Williams, J. A. G. *Dalton Trans.* **2002**, 1918. (d) Lazarides, T.; Alamiry, M. A. H.; Adams, H.; Pope, S. J. A.; Faulkner, S.; Weinstein, J. A.; Ward, M. D. *Dalton Trans.* **2007**, 1484. (e) Lazarides, T.; Tart, N. M.; Sykes, D.; Faulkner, S.; Barbieri, A.; Ward, M. D. *Dalton Trans.* **2009**, 3971.

(40) Rehm, D.; Weller, A. *Isr. J. Chem.* **1970**, *8*, 259.

(41) (a) Belser, P.; von Zelewsky, A. *Helv. Chim. Acta* **1980**, *63*, 1675. (b) Juris, A.; Balzani, V.; Barigelletti, F.; Campagna, S.; Belser, P.; von Zelewsky, A. *Coord. Chem. Rev.* **1988**, *84*, 85.